Research Article Vol. 2, No. 6 / June 2015 / Optica 530

On-chip mode-division multiplexing switch

Brian Stern,[1] Xiaoliang Zhu,[2] Christine P. Chen,[2] Lawrence D. Tzuang,[1] Jaime Cardenas,[1] Keren Bergman,[2] and Michal Lipson[1,*]

[1]School of Electrical and Computer Engineering, Cornell University, Ithaca, New York 14853, USA
[2]Department of Electrical Engineering, Columbia University, New York, New York 10027, USA
[3]Kavli Institute at Cornell for Nanoscale Science, Cornell University, Ithaca, New York 14853, USA
*Corresponding author: ml292@cornell.edu

Received 2 March 2015; revised 14 May 2015; accepted 15 May 2015 (Doc. ID 235401); published 1 June 2015

Leveraging the spatial modes of multimode waveguides using mode-division multiplexing on an integrated photonic chip allows unprecedented scaling of bandwidth density for on-chip communication. Switching channels between waveguides is critical for future scalable optical networks, but its implementation in multimode waveguides must address how to simultaneously control modes with vastly different optical properties. Here we present a platform for switching signals between multimode waveguides based on individually processing the spatial mode channels using single-mode elements. Using this wavelength-division multiplexing-compatible platform, we demonstrate a 1 × 2 multimode switch for a silicon chip that routes four data channels with low (< −16.8 dB) crosstalk. We show bit-error rates below 10^{-9} and power penalties below 1.4 dB on all channels while routing 10 Gb/s data when each channel is input and routed separately. The switch exhibits an additional power penalty of less than 2.4 dB when all four channels are simultaneously routed. These results enable individual processing of multimode signals and high-bandwidth, flexible optical networks.

OCIS codes: (130.3120) Integrated optics devices; (130.4815) Optical switching devices.

http://dx.doi.org/10.1364/OPTICA.2.000530

1. INTRODUCTION

Mode-division multiplexing (MDM) offers a new dimension to scale on-chip bandwidth by utilizing the spatial modes of waveguides to carry multiple optical signals simultaneously [1–21]. The ability to switch and route such channels through a reconfigurable network would enable new functionalities for MDM, which, when combined with wavelength-division multiplexing (WDM), has been projected to allow over 4 Tbps data rate on a single multimode waveguide [18]. However, switching has only been achieved in single-mode on-chip networks [22–27]. The difficulty in implementing switching for multimode waveguides is due to the contradictory design requirements: since the mode confinements in a multimode waveguide vary significantly between the different modes, the dimensions of the photonic structure required to perform the switching differ greatly from mode to mode as well. In fiber communication, despite the fact that spatial multiplexing has allowed enormous data rates over kilometers of fiber [28–38], its small index contrast ($\Delta n \sim 5 \times 10^{-3}$) makes coupling between modes rather strong, and therefore, modes are not easily separable and switching is confined only to the wavelength domain [39–43]. In integrated silicon waveguides, due to the much higher index contrast ($\Delta n \sim 2$), coupling between modes is much weaker, and therefore, an integrated multimode platform could allow arbitrary access to individual spatial modes and wavelengths alike to enable reconfigurable switching [44,45] for fully flexible, dense, on-chip optical networks. In this paper, we present an integrated multimode switch and demonstrate routing for simultaneous MDM and WDM on-chip. The switch routes four 10 Gb/s data channels independently between multimode waveguides with less than −16 dB measured crosstalk between modes.

2. PROCESSING MULTIMODE SIGNALS

We propose a platform for active, integrated multimode photonics based on the independent processing of the spatial modes' signals using single-mode elements. This approach leverages the high index contrast on-chip, which in turn enables access to the individual modes. In the proposed platform, the input multimode signals are first all converted into the fundamental mode, as illustrated in step (1) in Fig. 1 for the example case of 12 channels, consisting of three modes and four wavelengths. Once the modes are converted, processing of individual channels, now all accessible, regardless of mode or wavelength, is possible, including variable attenuation [step (2) in Fig. 1], switching, or modulation. Following the processing step, the channels are then reconverted into their original spatial modes at the output [step (3) in Fig. 1].

3. MULTIMODE SWITCH

As an example of the proposed platform, we show a multimode 1 × 2 switch for a silicon chip that supports four data channels,

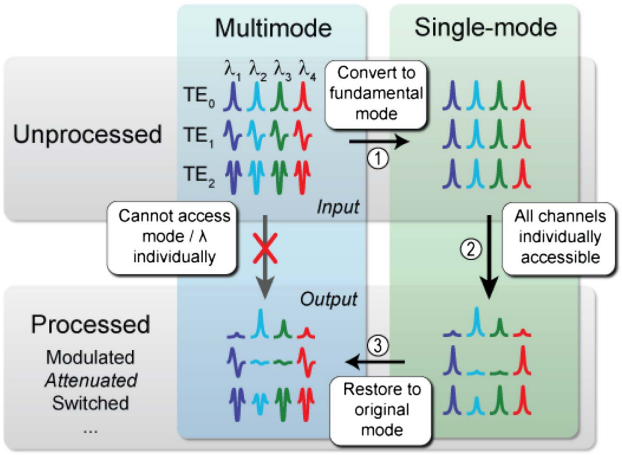

Fig. 1. In order to enable access to individual mode-multiplexed channels, multimode signals are temporarily encoded as the fundamental mode [step (1)] and are then processed independently [step (2)]. Processing by variable attenuation is shown as an example for the case of 12 channels (three modes and four wavelengths). Finally, the channels are restored as higher-order spatial modes [step (3)] and are coupled to a multimode waveguide output.

based on ring resonators for switching and for converting the different modes and wavelengths. The switch routes four channels, consisting of two transverse electric modes, TE_0 (fundamental) and TE_1, at two wavelengths near 1550 nm, from a single input to either of the two output ports [Fig. 2(a)]. Each of the four channels can be routed independently of each other for full switching selectivity. An example switching configuration is shown in Fig. 2(b). In order to convert all channels into the fundamental mode and back [stages (1) and (3) in Fig. 2(b)], we optimize the waveguide widths to ensure phase matching between the different modes in the waveguides: the TE_1 in the 930 nm wide multimode bus waveguide and the TE_0 in the 450 nm wide single-mode waveguides. We utilize racetrack ring resonators, as shown in Fig. 2(c), to enhance the coupling between these modes for efficient conversion within a short coupling section, as demonstrated in our previous work [18]. The design process for the parameters and the dimensions of the waveguides and rings are detailed further in Supplement 1. The switching backbone [stage (2) in Fig. 2(b)] also consists of ring resonators to allow compact, active control by integrated heaters [46]. These rings have a smaller radius of 8.6 μm [for a free spectral range (FSR) of 10 nm] and are only tuned into resonance when the desired channel is set to be switched, in contrast to the rings employed for mode conversion, which have a larger 16 μm radius (for a FSR of 5 nm) and are always kept tuned on resonance so that at all wavelengths the channels are converted between modes [47]. Note that, in principle, increasing the number of rings used for switching and tripling, quadrupling, etc., the FSRs of the rings used for conversion would enable additional wavelength channels.

4. DEVICE FABRICATION

We demonstrate the switch using high-index-contrast silicon waveguides fabricated on a silicon-on-insulator wafer with a 250-nm-thick silicon device layer on 3 μm buried oxide. The waveguides are patterned using electron beam lithography and fully etched using reactive-ion etching. The devices are then clad with 1 μm of plasma-enhanced chemical vapor deposition SiO_2. A thin Cr adhesion layer and 100 nm of Ni are evaporated along with a lift-off process to define the heaters for tuning resonances. For the metal contacts, 1.7 μm of Al is sputtered with a thin Ti adhesion layer and then etched using inductively coupled plasma. Deep trenches are etched into the silicon substrate near the input and output waveguide tapers for improved coupling [48,49].

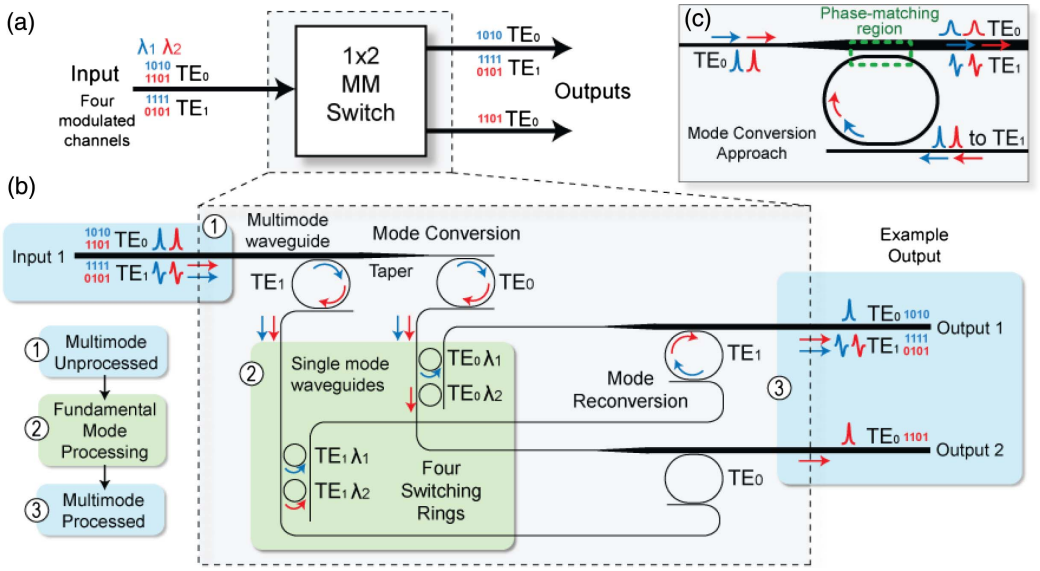

Fig. 2. (a) Block diagram of 1 × 2 multimode switch operation. The four input data channels, consisting of two modes at two different wavelengths, may be switched in any combination to the two outputs. The example shows three channels routed to Output 1 and one channel to Output 2. (b) Schematic of the multimode switch. The input TE_1 channels are converted to the fundamental mode through phase matching to single-mode rings. The channels are switched using actively tuned rings to route them individually. This example shows three channels routed from Input 1 to Output 1 using on-resonance rings, and the fourth channel ($TE_0\lambda_2$) is routed from Input 1 to Output 2 using an off-resonance ring. (c) Illustration of the mode (re)conversion approach showing the phase-matched coupling region.

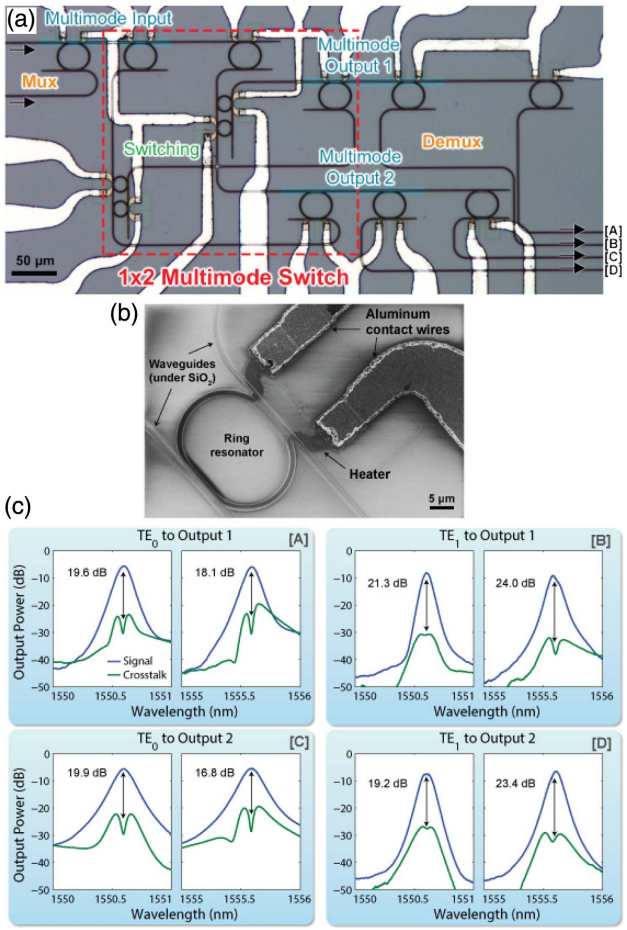

Fig. 3. (a) Optical microscope image of the fabricated device. The input channels are coupled into single-mode waveguides from an off-chip laser and a multiplexer (mux) produces the MDM input to the multimode switch. The areas highlighted in blue show the multimode waveguides. The four small rings actively switch the four channels and are tuned by integrated heaters. Following the switch, each of the two outputs is demultiplexed (demux) so that the channels can be individually monitored off-chip. (b) SEM image of a ring resonator in the fabricated device with active heater used to tune the resonance. (c) Crosstalk measurements for the different channels. Spectral profiles at both outputs for each of the four input channels, compared with profiles from interfering channels. Signal and crosstalk were measured individually with a continuous-wave tunable laser for configurations with the highest intermodal crosstalk, which remain below −16.8 dB in all cases.

The final chip is mounted to a custom printed circuit board, onto which the Al pads are wirebonded out for easy control of heater tuning by DC voltages. Figures 3(a) and 3(b) show microscope and scanning electron microscope images of the on-chip multimode switch. The switch area is less than 0.07 mm^2, and an even more compact design could be achieved by using smaller tapers or by placing the components closer together.

5. RESULTS

We measure less than −16.8 dB crosstalk when switching each of the four individual channels to the different output ports. In order to couple on and off the chip using single-mode edge coupling based on an inverted taper [49], a mode (de)multiplexer is added to the input (outputs) of the switch [18]. We measure the intermodal crosstalk between channels by launching one channel at a time and detecting the power within the channel's bandwidth at each output to compare the desired signal with leaked, interfering signals from other channels [Fig. 3(c)]. For all channels and switching configurations, this crosstalk remains low, ranging from −16.8 to −24.0 dB for each channel. These crosstalk values are comparable to those of previous integrated multimode multiplexer systems [10,13,18], indicating that the switch introduces negligible crosstalk. The measured insertion loss, including on- and off-chip coupling losses, is 5.4–9.1 dB for the four different channels. Based on the measured losses from test structures that do not include the switch or multiplexers, we estimate the losses due to the switch and multiplexers together to be between 0.9 and 4.6 dB. This mode-dependent insertion loss is likely due to variations in the rings' coupling (and therefore, extinction ratio [50]) and also a result of narrowing bandwidth after multiple conversion steps, which leads to greater losses for the higher-order modes in this case. The extinction ratio can in principle be improved using tunable couplers such as interferometers on the single-mode coupling regions of the rings [51], and a wider bandwidth for the rings through stronger coupling can prevent accumulated loss during each conversion step.

Our 1×2 multimode switch exhibits bit-error rates (BERs) below 10^{-9} on all channels and open eye diagrams while routing 10 Gb/s data when each channel is input and routed separately. We perform the experiment using a tunable laser modulated by a pseudo-random binary sequence (PRBS) from a pattern generator [Fig. 4(a)]. The modulated light is coupled onto the chip using a tapered fiber. A DC voltage is applied to each integrated heater to align their resonances with the laser or to tune and detune the resonances of the rings used for switching to route the channels to the outputs. The total power supplied to the heaters is up to 30 mW, depending on the switching state, and is almost entirely used for aligning the resonances of all rings due to fabrication variations. A back-to-back reference for the transmission experiment is measured for each wavelength by removing the chip and replacing the tapered fibers with a single fiber connection. The output signal from the chip is amplified and filtered (to reject amplified spontaneous emission noise) to obtain optical eye diagrams of the transmitted data pattern [Fig. 4(b)]. One can see that the signals exhibit open eye diagrams for all four channels routed to either output. We further characterize the data integrity with BER measurements [Fig. 4(c)]. We measure error-free switching (BER $< 10^{-9}$) for all channels, with power penalty ranging between 0.5 and 1.0 dB for TE_0 and 1.2 and 1.4 dB for TE_1.

The switch exhibits an additional power penalty of less than 2.4 dB when all four channels are simultaneously inserted onto the chip and routed. In order to accommodate two wavelength channels (λ_1 and λ_2), we decorrelate them using 500 m of single-mode fiber and then combine and split them equally on two paths [Fig. 5(a)]. Another length of 2 km of fiber on one path ensures the phase decoherence of the two paths, as it is several times the laser coherence length of 450 m. Each path has equal power and is coupled simultaneously into the TE_0 and TE_1 inputs using a pitch-reducing optical fiber array (PROFA) [52]. A tapered fiber is used to selectively measure the outputs of the chip by mode and the tunable filter is aligned to measure by wavelength channel. We observe open eye diagrams for the four simultaneously routed 10 Gb/s channels [Fig. 5(b)]. The back-to-back references are measured by replacing the chip and the PROFA

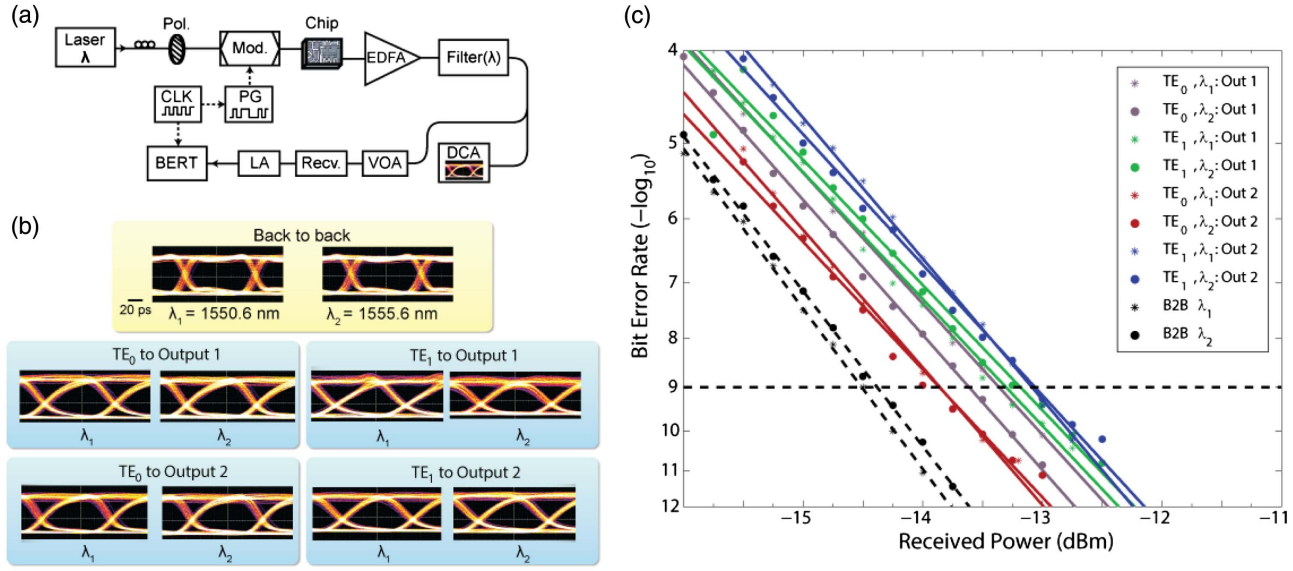

Fig. 4. (a) Testing configuration including a tunable laser, a polarization controller, a fiber polarizer, an electro-optic modulator (Mod.), a pattern generator (PG) for the 2^7–1 PRBS, a function generator clock source (CLK), an Er-doped fiber amplifier (EDFA), a tunable bandpass filter (1.4 nm), a digital communications analyzer (DCA), a variable optical attenuator (VOA), an optical receiver (Recv.), a limiting amplifier (LA), and a BER tester (BERT). (b) Eye diagrams of the switched signals for all channels at both outputs are open. Comparison with the rise time of back-to-back eyes confirms that the output signal is bandwidth-limited. (c) Error-free transmission (BER $< 10^{-9}$) is achieved, with power penalties ranging from 0.5 to 1.4 dB, compared with the back-to-back (B2B) references.

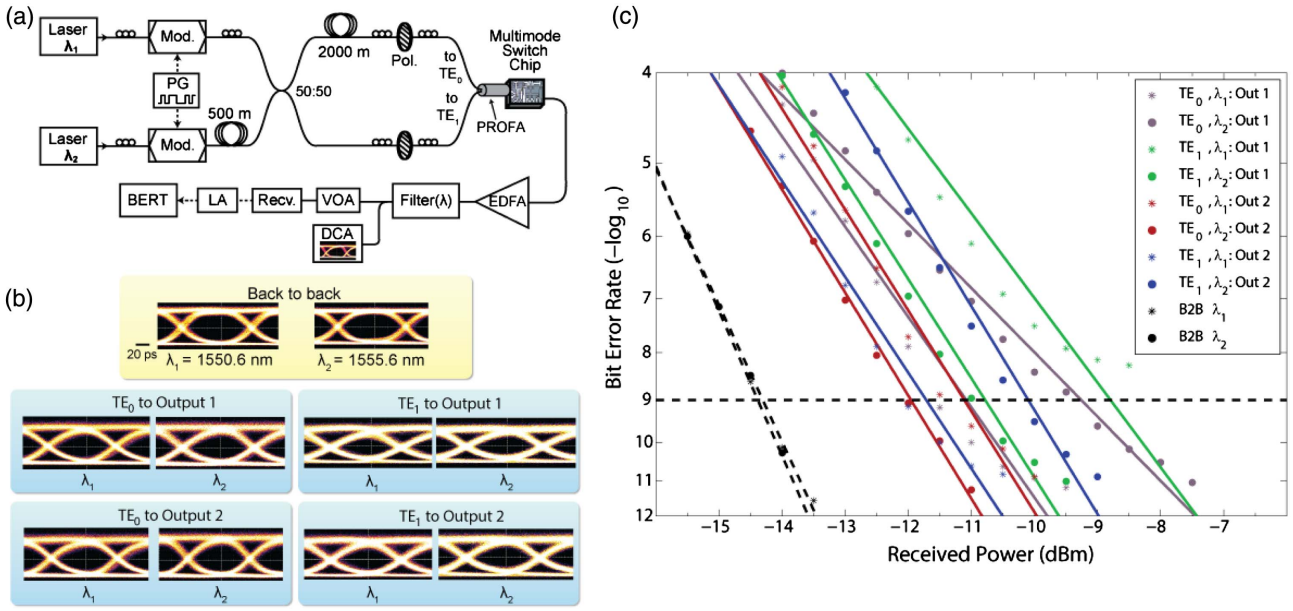

Fig. 5. (a) Testing setup for simultaneous switching, derived from that in Fig. 4(a), including fiber spools for decorrelation and decoherence of data channels, a 50:50 combiner/splitter, and a PROFA. The solid connections are in fiber and the dotted connections are electrical. (b) Eye diagrams for each 10 Gb/s channel switching to either output. (c) BER measurements for simultaneous operation of all channels. The worst-case switching configuration for each channel is plotted. For each channel, a back-to-back reference was measured by replacing the PROFA and the chip with an attenuator replicating the insertion loss. The best-performing back-to-back measurements for each wavelength are plotted. All channels achieve error-free (BER $< 10^{-9}$) transmission except the $TE_1\lambda_1$ channel, which is impaired when switched to Output 1 due to fabrication error causing one ring resonator to be undercoupled with a narrow bandwidth.

with an attenuator to replicate each path's insertion loss. We also measure the BERs for all channels [Fig. 5(c)] for the highest-crosstalk configuration, i.e., when the mode channels are routed to the same output. We observe power penalties of 2.4–5.1 dB for simultaneous operation and error-free switching (BER $< 10^{-9}$) for all channels except $TE_1\lambda_1$ at Output 1, which reaches 5×10^{-9}. The additional power penalty of 1.8–2.4 dB due to simultaneous operation could be minimized by optimizing the bandwidth of each ring to equalize the effect of intrachannel crosstalk among the different paths. The higher power penalty

for channel $TE_1\lambda_1$ at Output 1 is due to fabrication error causing one switching ring to be undercoupled, resulting in a narrow bandwidth of only 9 GHz, compared with the larger bandwidth for the other channels of approximately 13 GHz.

6. DISCUSSION

This demonstration of, to the best of our knowledge, the first integrated multimode switch establishes MDM as a viable platform for optical interconnects. It allows the scaling of bandwidth density for on-chip networks by expanding routing to include waveguides employing simultaneous MDM and WDM for multidimensional multiplexing. The ability to route on-chip MDM–WDM signals with full flexibility enables integrated networks with many nodes connected by high-bandwidth multimode links to dynamically allocate bandwidth. While each multimode input or output in this demonstration carries 40 Gb/s aggregate bandwidth (4×10 Gb/s), the design is scalable in principle to more modes and wavelengths. In addition, the switching design can be optimized to accommodate higher data rates such as 25 Gb/s at the expense of fewer wavelength channels while still reaching similar aggregate bandwidths. In principle, one can also use MDM channels to reduce the number of independent laser sources required. Because lasers are the dominant cause of power consumption in WDM systems [53], mode channels can also significantly reduce power consumption. The platform we present for processing multimode signals in the single-mode domain also creates the possibility for numerous future applications of MDM beyond routing, such as modulation, attenuation, or performance monitoring.

National Science Foundation (NSF) - CIAN ERC (EEC-0812072).

This work was performed in part at the Cornell NanoScale Facility, a member of the National Nanotechnology Infrastructure Network, which is supported by the National Science Foundation (NSF) through grant ECCS-0335765, and made use of the Cornell Center for Materials Research Shared Facilities, which are supported through the NSF MRSEC program (DMR-1120296). The authors also acknowledge the NSF GRFP and Intel SRC Ph.D. Fellowship.

See Supplement 1 for supporting content.

REFERENCES

1. B.-T. Lee and S.-Y. Shin, "Mode-order converter in a multimode waveguide," Opt. Lett. **28**, 1660–1662 (2003).
2. M. Greenberg and M. Orenstein, "Multimode add-drop multiplexing by adiabatic linearly tapered coupling," Opt. Express **13**, 9381–9387 (2005).
3. S. Bagheri and W. M. J. Green, "Silicon-on-insulator mode-selective add-drop unit for on-chip mode-division multiplexing," in *6th IEEE International Conference on Group IV Photonics, 2009 (GFP '09)*, San Francisco, California, September 9–11, 2009, pp. 166–168.
4. A. C. Ruege and R. M. Reano, "Multimode waveguides coupled to single mode ring resonators," J. Lightwave Technol. **27**, 2035–2043 (2009).
5. L. H. Frandsen, Y. Elesin, L. F. Frellsen, M. Mitrovic, Y. Ding, O. Sigmund, and K. Yvind, "Topology optimized mode conversion in a photonic crystal waveguide fabricated in silicon-on-insulator material," Opt. Express **22**, 8525–8532 (2014).
6. M. Heinrich, M.-A. Miri, S. Stützer, R. El-Ganainy, S. Nolte, A. Szameit, and D. N. Christodoulides, "Supersymmetric mode converters," Nat. Commun. **5**, 3698 (2014).
7. N. Hanzawa, K. Saitoh, T. Sakamoto, T. Matsui, K. Tsujikawa, M. Koshiba, and F. Yamamoto, "Mode multi/demultiplexing with parallel waveguide for mode division multiplexed transmission," Opt. Express **22**, 29321–29330 (2014).
8. W. Chen, P. Wang, and J. Yang, "Mode multi/demultiplexer based on cascaded asymmetric Y-junctions," Opt. Express **21**, 25113–25119 (2013).
9. C. P. Chen, J. Driscoll, B. Souhan, R. Grote, X. Zhu, R. M. Osgood, and K. Bergman, "Experimental demonstration of spatial scaling for high-throughput transmission through a Si mode-division-multiplexing waveguide," in *Advanced Photonics for Communications*, OSA Technical Digest (online) (Optical Society of America, 2014), paper IM2A.3.
10. J. B. Driscoll, R. R. Grote, B. Souhan, J. I. Dadap, M. Lu, and R. M. Osgood, "Asymmetric Y junctions in silicon waveguides for on-chip mode-division multiplexing," Opt. Lett. **38**, 1854–1856 (2013).
11. J. B. Driscoll, C. P. Chen, R. R. Grote, B. Souhan, J. I. Dadap, A. Stein, M. Lu, K. Bergman, and R. M. Osgood, "A 60 Gb/s MDM–WDM Si photonic link with < 0.7 dB power penalty per channel," Opt. Express **22**, 18543–18555 (2014).
12. T. Uematsu, Y. Ishizaka, Y. Kawaguchi, K. Saitoh, and M. Koshiba, "Design of a compact two-mode multi/demultiplexer consisting of multimode interference waveguides and a wavelength-insensitive phase shifter for mode-division multiplexing transmission," J. Lightwave Technol. **30**, 2421–2426 (2012).
13. J. Wang, P. Chen, S. Chen, Y. Shi, and D. Dai, "Improved 8-channel silicon mode demultiplexer with grating polarizers," Opt. Express **22**, 12799–12807 (2014).
14. J. Wang, S. Chen, P. Chen, Y. Shi, and D. Dai, "64-channel hybrid (de) multiplexer enabling wavelength- and mode-division multiplexing for on-chip optical interconnects," in *Asia Communications and Photonics Conference 2014*, OSA Technical Digest (online) (Optical Society of America, 2014), paper ATh1A.7.
15. M. Yin, Q. Deng, Y. Li, X. Wang, and H. Li, "Compact and broadband mode multiplexer and demultiplexer based on asymmetric plasmonic–dielectric coupling," Appl. Opt. **53**, 6175–6180 (2014).
16. Y. Ding, J. Xu, F. Da Ros, B. Huang, H. Ou, and C. Peucheret, "On-chip two-mode division multiplexing using tapered directional coupler-based mode multiplexer and demultiplexer," Opt. Express **21**, 10376–10382 (2013).
17. Y.-D. Yang, Y. Li, Y.-Z. Huang, and A. W. Poon, "Silicon nitride three-mode division multiplexing and wavelength-division multiplexing using asymmetrical directional couplers and microring resonators," Opt. Express **22**, 22172–22183 (2014).
18. L.-W. Luo, N. Ophir, C. P. Chen, L. H. Gabrielli, C. B. Poitras, K. Bergmen, and M. Lipson, "WDM-compatible mode-division multiplexing on a silicon chip," Nat. Commun. **5**, 3069 (2014).
19. T. Mulugeta and M. Rasras, "Silicon hybrid (de)multiplexer enabling simultaneous mode and wavelength-division multiplexing," Opt. Express **23**, 943–949 (2015).
20. B. A. Dorin and W. N. Ye, "Two-mode division multiplexing in a silicon-on-insulator ring resonator," Opt. Express **22**, 4547–4558 (2014).
21. H. Chen, R. van Uden, C. Okonkwo, and T. Koonen, "Compact spatial multiplexers for mode division multiplexing," Opt. Express **22**, 31582–31594 (2014).
22. V. R. Almeida, C. A. Barrios, R. R. Panepucci, and M. Lipson, "All-optical control of light on a silicon chip," Nature **431**, 1081–1084 (2004).
23. P. Dong, S. F. Preble, and M. Lipson, "All-optical compact silicon comb switch," Opt. Express **15**, 9600–9605 (2007).
24. M. Yang, W. M. J. Green, S. Assefa, J. Van Campenhout, B. G. Lee, C. V. Jahnes, F. E. Doany, C. L. Schow, J. A. Kash, and Y. A. Vlasov, "Non-blocking 4 × 4 electro-optic silicon switch for on-chip photonic networks," Opt. Express **19**, 47–54 (2011).
25. R. Ji, L. Yang, L. Zhang, Y. Tian, J. Ding, H. Chen, Y. Lu, P. Zhou, and W. Zhu, "Five-port optical router for photonic networks-on-chip," Opt. Express **19**, 20258–20268 (2011).
26. A. Biberman, K. Preston, G. Hendry, N. Sherwood-Droz, J. Chan, J. S. Levy, M. Lipson, and K. Bergman, "Photonic network-on-chip architectures using multilayer deposited silicon materials for high-performance chip multiprocessors," J. Emerg. Technol. Comput. Syst. **7**, 1–25 (2011).
27. B. G. Lee, A. V. Rylyakov, W. M. J. Green, S. Assefa, C. W. Baks, R. Rimolo-Donadio, D. M. Kuchta, M. H. Khater, T. Barwicz, C. Reinholm, E. Kiewra, S. M. Shank, C. L. Schow, and Y. A. Vlasov, "Monolithic silicon integration of scaled photonic switch fabrics,

CMOS logic, and device driver circuits," J. Lightwave Technol. **32**, 743–751 (2014).
28. D. J. Richardson, J. M. Fini, and L. E. Nelson, "Space-division multiplexing in optical fibres," Nat. Photonics **7**, 354–362 (2013).
29. P. J. Winzer, "Making spatial multiplexing a reality," Nat. Photonics **8**, 345–348 (2014).
30. K. Igarashi, T. Tsuritani, I. Morita, Y. Tsuchida, K. Maeda, M. Tadakuma, T. Saito, K. Watanabe, K. Imamura, R. Sugizaki, and M. Suzuki, "Super-Nyquist-WDM transmission over 7,326-km seven-core fiber with capacity-distance product of 1.03 Exabit/s·km," Opt. Express **22**, 1220–1228 (2014).
31. J. Sakaguchi, B. J. Puttnam, W. Klaus, Y. Awaji, N. Wada, A. Kanno, T. Kawanishi, K. Imamura, H. Inaba, K. Mukasa, R. Sugizaki, T. Kobayashi, and M. Watanabe, "305 Tb/s space division multiplexed transmission using homogeneous 19-core fiber," J. Lightwave Technol. **31**, 554–562 (2013).
32. R. G. H. van Uden, R. A. Correa, E. A. Lopez, F. M. Huijskens, C. Xia, G. Li, A. Schülzgen, H. de Waardt, A. M. J. Koonen, and C. M. Okonkwo, "Ultra-high-density spatial division multiplexing with a few-mode multicore fibre," Nat. Photonics **8**, 865–870 (2014).
33. N. Amaya, M. Irfan, G. Zervas, R. Nejabati, D. Simeonidou, J. Sakaguchi, W. Klaus, B. J. Puttnam, T. Miyazawa, Y. Awaji, N. Wada, and I. Henning, "Fully-elastic multi-granular network with space/frequency/time switching using multi-core fibres and programmable optical nodes," Opt. Express **21**, 8865–8872 (2013).
34. H. Takara, A. Sano, T. Kobayashi, H. Kubota, H. Kawakami, A. Matsuura, Y. Miyamoto, Y. Abe, H. Ono, K. Shikama, Y. Goto, K. Tsujikawa, Y. Sasaki, I. Ishida, K. Takenaga, S. Matsuo, K. Saitoh, M. Koshiba, and T. Morioka, "1.01-Pb/s (12 SDM/222 WDM/456 Gb/s) crosstalk-managed transmission with 91.4-b/s/Hz aggregate spectral efficiency," in *European Conference and Exhibition on Optical Communication*, OSA Technical Digest (online) (Optical Society of America, 2012), paper Th.3.C.1.
35. N. K. Fontaine, C. R. Doerr, M. A. Mestre, R. Ryf, P. Winzer, L. Buhl, Y. Sun, X. Jiang, and R. Lingle, "Space-division multiplexing and all-optical MIMO demultiplexing using a photonic integrated circuit," in *Optical Fiber Communication Conference*, OSA Technical Digest (Optical Society of America, 2012), paper PDP5B.1.
36. S. Randel, R. Ryf, A. Sierra, P. J. Winzer, A. H. Gnauck, C. A. Bolle, R.-J. Essiambre, D. W. Peckham, A. McCurdy, and R. Lingle, "6 × 56-Gb/s mode-division multiplexed transmission over 33-km few-mode fiber enabled by 6 × 6 MIMO equalization," Opt. Express **19**, 16697–16707 (2011).
37. R. Ryf, S. Randel, A. H. Gnauck, C. Bolle, A. Sierra, S. Mumtaz, M. Esmaeelpour, E. C. Burrows, R. Essiambre, P. J. Winzer, D. W. Peckham, A. H. McCurdy, and R. Lingle, "Mode-division multiplexing over 96 km of few-mode fiber using coherent 6 × 6 MIMO processing," J. Lightwave Technol. **30**, 521–531 (2012).
38. R. Ryf, N. K. Fontaine, H. Chen, B. Guan, B. Huang, M. Esmaeelpour, A. H. Gnauck, S. Randel, S. J. B. Yoo, A. M. J. Koonen, R. Shubochkin, Y. Sun, and R. Lingle, "Mode-multiplexed transmission over conventional graded-index multimode fibers," Opt. Express **23**, 235–246 (2015).
39. K.-P. Ho, J. M. Kahn, and J. P. Wilde, "Wavelength-selective switches for mode-division multiplexing: scaling and performance analysis," J. Lightwave Technol. **32**, 3724–3735 (2014).
40. R. Ryf, N. K. Fontaine, J. Dunayevsky, D. Sinefeld, M. Blau, M. Montoliu, S. Randel, C. Liu, B. Ercan, M. Esmaeelpour, S. Chandrasekhar, A. H. Gnauck, S. G. Leon-Saval, J. Bland-Hawthorn, J. R. Salazar-Gil, Y. Sun, L. Gruner-Nielsen, R. Lingle, and D. M. Marom, "Wavelength-selective switch for few-mode fiber transmission," in *39th European Conference and Exhibition on Optical Communication (ECOC 2013)*, London, UK, September 22–26, 2013, pp. 1–3.
41. X. Chen, A. Li, J. Ye, A. Al Amin, and W. Shieh, "Demonstration of few-mode compatible optical add/drop multiplexer for mode-division multiplexed superchannel," J. Lightwave Technol. **31**, 641–647 (2013).
42. R. Y. Gu, E. Ip, M.-J. Li, Y.-K. Huang, and J. M. Kahn, "Experimental demonstration of a spatial light modulator few-mode fiber switch for space-division multiplexing," in *Frontiers in Optics 2013 Postdeadline*, Orlando, Florida, October 6–10, 2013.
43. J. A. Carpenter, S. G. Leon-Saval, J. R. Salazar Gil, J. Bland-Hawthorn, G. Baxter, L. Stewart, S. Frisken, M. A. Roelens, B. J. Eggleton, and J. Schröder, "1 × 11 few-mode fiber wavelength selective switch using photonic lanterns," in *Optical Fiber Communication Conference*, OSA Technical Digest (online) (Optical Society of America, 2014), paper Th4A.2.
44. M. Cvijetic, I. B. Djordjevic, and N. Cvijetic, "Dynamic multidimensional optical networking based on spatial and spectral processing," Opt. Express **20**, 9144–9150 (2012).
45. D. Dai, J. Wang, and S. He, "Silicon multimode photonic integrated devices for on-chip mode-division-multiplexed optical interconnects," Prog. Electromagn. Res. **143**, 773–819 (2013).
46. N. Sherwood-Droz, H. Wang, L. Chen, B. G. Lee, A. Biberman, K. Bergman, and M. Lipson, "Optical 4 × 4 hitless silicon router for optical networks-on-chip (NoC)," Opt. Express **16**, 15915–15922 (2008).
47. J. Chan, N. Ophir, C. P. Lai, A. Biberman, H. L. R. Lira, M. Lipson, and K. Bergman, "Data transmission using wavelength-selective spatial routing for photonic interconnection networks," in *Optical Fiber Communication Conference/National Fiber Optic Engineers Conference 2011*, OSA Technical Digest (CD) (Optical Society of America, 2011), paper OThQ3.
48. J. Cardenas, C. B. Poitras, K. Luke, L. Luo, P. A. Morton, and M. Lipson, "High coupling efficiency etched facet tapers in silicon waveguides," IEEE Photon. Technol. Lett. **26**, 2380–2382 (2014).
49. V. R. Almeida, R. R. Panepucci, and M. Lipson, "Nanotaper for compact mode conversion," Opt. Lett. **28**, 1302–1304 (2003).
50. A. Yariv, "Universal relations for coupling of optical power between microresonators and dielectric waveguides," Electron. Lett. **36**, 321–322 (2000).
51. L.-W. Luo, S. Ibrahim, A. Nitkowski, Z. Ding, C. B. Poitras, S. J. Ben Yoo, and M. Lipson, "High bandwidth on-chip silicon photonic interleaver," Opt. Express **18**, 23079–23087 (2010).
52. V. I. Kopp, J. Park, M. Wlodawski, J. Singer, D. Neugroschl, and A. Z. Genack, "Pitch reducing optical fiber array for dense optical interconnect," in *2012 IEEE Avionics, Fiber-Optics and Photonics Technology Conference (AVFOP)*, Cocoa Beach, Florida, September 11–13, 2012, pp. 48–49.
53. R. Hendry, D. Nikolova, S. Rumley, N. Ophir, and K. Bergman, "Physical layer analysis and modeling of silicon photonic WDM bus architectures," in *HiPEAC*, Vienna, Austria, January, 2014.